Streamer initiation in atmospheric pressure gas discharges by direct particle simulation

B. J. P. Dowds, R. K. Barrett, and D. A. Diver
Department of Physics and Astronomy, University of Glasgow, Glasgow G12 8QQ, United Kingdom
(Received 11 April 2003; published 22 August 2003)

A two-dimensional particle code that simulates electrical breakdown of gases by modeling avalanche evolution from the initial ion-electron pair up to the development of a streamer is presented. Trajectories of individual particles are followed, the self-field is included consistently and collision processes are accurately modeled using experimentally determined cross sections. It is emphasized that the tadpolelike structure of well-formed streamer heads is present throughout the avalanche phase, and that the transition to the self-similar evolution characteristic of the streamer phase merely reflects the continued development of this structure. The importance of this for conventional fluid simulations of streamers, where the initial conditions for the streamer are taken to be a structureless Gaussian concentration of neutral plasma with significant density, is discussed. In the (realistic) situation where several avalanches are present simultaneously the large self-fields that rapidly develop lead to a strong interaction between them, in accord with the standard ''cartoon'' of streamer evolution.

DOI: 10.1103/PhysRevE.68.026412 PACS number(s): 51.50.+v, 34.80.Dp, 52.25.Jm, 52.65.Cc

I. INTRODUCTION

Since Raether [1,2] and Loeb and Meek [3] first introduced the streamer mechanism for electrical breakdown of gases, the subject has received increasing attention, both experimentally and theoretically. However, due to the extremely short time scales involved it has proved difficult to quantify and model the properties of streamers.

Streamers occur when an ionization avalanche formed from the acceleration of a seed ion-electron pair in the applied field grows to the point where the self-field produced by the space charge becomes comparable to the applied field [4]. Essentially, individual electrons are accelerated by the applied field until they gain sufficient energy to ionize a neutral gas atom. With each set of collisions the number of charged particles doubles, resulting in an avalanche (a Townsend cascade) where the numbers of charged particles and their density grow exponentially. A general introduction to electrical breakdowns and gas discharges is given in Ref. [5], a comprehensive review of previous gas discharge models is contained in Ref. [6], and extensive literature on these subjects exists [7–11].

Our current theoretical understanding of electrical breakdown in gas discharges is largely based on two-component fluid modeling of the streamer phase [12–17]. The majority of research has focused on anode directed streamers initiated on or close to the cathode, although cathode directed streamers have also been studied [12,16]. Recent experimental results [18,19] show that there remain discrepancies between simulations and laboratory measurements.

In fluid simulations of streamers several simplifying assumptions are usually made. First, the initial distribution of plasma is commonly taken to be a Gaussian concentration of neutral plasma with a particle density corresponding to the estimated avalanche density ($\sim 10^{14}$ cm^{-3}) at the avalanche-to-streamer transition [12–14]. The avalanche is not itself modeled, so its structure at the avalanche-to-streamer transition is not known, and is assumed to be unimportant for the subsequent development of the streamer. This overlooks the fact that the avalanche already has structure within it: the ionization front is present, charge separation has been set up, and there is a self-field that grows in concert with the particle densities (see Figs. 8 and 5). The importance of this for streamer development and modeling in the fluid approximation is discussed below.

Second, fluid simulations assume an initial level of background ionization (particle densities in the range from 1 cm^{-3} to 10^8 cm^{-3}) throughout the discharge region. This is largely to ensure numerical stability as the streamer propagates into the empty region, but the level of background ionization chosen can have a significant effect on the streamer evolution. The physical justification for this background ionization is unclear, particularly as in some cases it amounts to less than one charged particle in the computational region. The use of a particle simulation to model the initial avalanche phase overcomes both of these problems, as no assumptions about the initial distribution of plasma in the particle code are made.

The particle model presented here realistically simulates an avalanche from the initial ion-electron pair up to and beyond the avalanche-to-streamer transition by following the trajectories of all particles in the avalanche through the total field, including the effects of elastic and inelastic collisions. Accurate determination of the charged-particle densities and self-potential along with important microphysical data can be obtained. The design of the particle code is such that it can interface easily with a fluid code for continued streamer evolution to time scales (and particle densities) impractical in a particle approach. Fluid simulations incorporating particle modeling do exist [20], but do not follow all the charged particles, including only a subset of the electrons. The authors can find no previously published work in which a solely particle model is used to simulate the avalanche phase.

Section II describes, in detail, the particle model. Section III presents the results of the model. Finally, Sec. IV contains our conclusions.

II. PARTICLE MODEL

Previous attempts at discharge models have employed fluid simulations [12,15,17,21]. In these simulations the ini-

tial conditions have been a neutral Gaussian plasma perturbation, which has then been evolved by the fluid code into a streamer. The particle model presented here makes no such assumption. Instead an initial ion-electron pair is placed in a parallel plate gap, containing a uniform stationary continuum of cold neutrals with which the electrons collide.

When a voltage of the order of the breakdown voltage for the gas is applied to the gap, the electron, being greatly more mobile than the ion, is rapidly accelerated towards the anode. It gains energy from the electric field, and is soon energetic enough so that a collision with a gas atom could liberate another electron, i.e., $K_e \geqslant e\varphi$ where K_e is the kinetic energy of the electron, e is the electric charge, and φ is the first-ionization potential for the gas. This liberation creates an additional ion-electron pair. The two electrons continue this process leading to an exponentially increasing number of both charged-particle species.

To model this exponential growth of charged-particle density produced by electron impact ionization, the trajectories of the individual electrons and ions are calculated. Furthermore, the self-field produced by the charges themselves is self-consistently taken into account throughout the simulation, by assigning space charge density to a grid and solving Poisson's equation for the self-potential at each time step using trigonometric Fourier transforms [22]. In this way we can include both Dirichlet and von Neumann boundary conditions.

After solving Poisson's equation, the particle trajectories are calculated by numerically integrating the differential form of the equations of motion by a standard fourth-order Runge Kutta technique. The relevant equations are

$$m_s \frac{d^2\mathbf{s}_s}{dt^2} = q_s\mathbf{E} - \mathcal{F}_{s,coll}, \tag{1}$$

$$\nabla^2\phi_{\text{self}} = -\frac{e}{\varepsilon_0}(n_i - n_e), \tag{2}$$

$$\mathbf{E}_{\text{self}} = -\nabla\phi_{\text{self}}, \tag{3}$$

$$\mathbf{E} = \mathbf{E}_{\text{app}} + \mathbf{E}_{\text{self}}, \tag{4}$$

where $\mathbf{s}_s$, m_s, and q_s are the vector displacement, mass and charge of species s and $\mathcal{F}_{s,coll}$ represents the effect of stochastic collisions (see the following section). ϕ_{self} is the self-potential, n_i and n_e are the ion and electron densities, respectively. $\mathbf{E}$, $\mathbf{E}_{\text{app}}$, and $\mathbf{E}_{\text{self}}$ are the total, applied, and self-field. Nondimensionalizing these equations results in the following nondimensional parameter below:

$$\Lambda = \frac{-eQn_xn_yn_{1\text{D}}}{\varepsilon_0 E_{\text{app}} x_{\text{gap}}}, \tag{5}$$

where n_x, n_y are the number of grid points in the x and y directions, respectively, and Q is the charge factor which is a measure of the number of charged particles that a given particle represents and $n_{1\text{D}}$ is a linear density that relates the nondimensionalized model densities to their dimensionalized counterparts. Q and $n_{1\text{D}}$ will be explained in more detail below.

The field at the particle is evaluated by a bilinear interpolation of the fields at the four surrounding grid points.

A. Collisions

In the work presented here only ionizing and elastic collisions are considered for simplicity, however it would be a simple extension of the code to incorporate other collision types.

Once an electron has enough energy to cause ionization it is considered to be a candidate for such a collision. The energy dependence of cross section used for ionizing collisions [23] is

$$\sigma_{iz}(\kappa) = \frac{1}{\kappa}\left[A\ln(\kappa) + \frac{B\ln(\kappa) + C(\kappa - 1)}{\kappa + D}\right],$$

where

$$\kappa = \frac{K}{K_{iz}} \quad \text{and} \quad \kappa \geqslant 1, \tag{6}$$

where K and K_{iz} are the energy of the impacting electron and the ionization energy of the atom.

The constants A, B, C, and D are obtained by fitting the formula to experimentally obtained data, from the National Institute of Standards and Technology (NIST) electron impact ionization cross section database [24]. Note that this has the correct form at high electron energies, $\sigma_{iz} \propto K^{-1}\ln(K)$ as predicted by quantum mechanical calculations; if the form of cross section, particularly at high energy, is incorrect the spatial distribution of the particles along with their energies is radically different. In order to achieve a distribution of random path lengths with the correct mean free path (MFP) λ we draw the actual path length for a particle from an exponential distribution with mean λ. (In practice, the energy dependence is folded into consideration of the MFP.)

The products of a ionizing collision are always two electrons (the original and the created) and one ion. Total energy, including ionization energy, and momentum are conserved in the collision. As no internal excitations are considered the energy available postcollision is one ionization energy less than that available precollision. The ion is given a random fraction of its maximum possible energy (the maximum value is dictated by the conservation equations). The remaining energy is split randomly between the two outgoing electrons. Fixing the outgoing ion direction and the angle between the outgoing electrons is then sufficient to determine fully the kinematics of the collision. For ionizing collisions we have assumed isotropic scattering of the charged particles: the outgoing ions are distributed uniformly in direction and the angle between the outgoing electrons is chosen uniformly over the range permitted by energy and momentum conservation.

Elastic collisions are included in a similar manner. We have taken the elastic collision cross section for nitrogen to be a constant, with a representative value of $\sigma_{el} = 1.0$

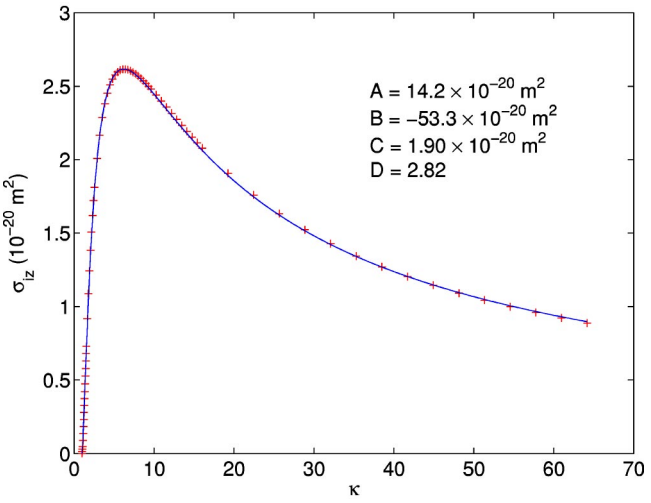

FIG. 1. The fit (solid line) of Eq. (6) to the NIST data (+).

$\times 10^{-19}$ m^2 [25]. Small variations in this parameter have a negligible effect on the streamer development and do not affect the conclusions we reach. Elastic collisions are not isotropic but have a preference to forward scattering [26]. In order to mimic suitably this behavior with minimal computational overhead, a simple form for the scattering angle θ, in the range $[-\pi,\pi]$, is used;

$$\theta = 8\pi\left(p-\frac{1}{2}\right)^3, \tag{7}$$

where p is a uniform random number between 0 and 1. When using this form $[C(p-1/2)^n]$, odd powers ensure the full $[-\pi,\pi]$ range without an extra computation.

There is no energy threshold for elastic collisions and the resulting trajectories of the neutrals are not followed.

B. Time steps

The size of the time step used is of crucial importance. Too small a time step is computationally impractical: too large a time step leads to a poorer resolution of the field structure because the particle trajectories are less accurately determined.

Given that the MFP is inversely proportional to the cross section, and the form of σ_{iz} from Eq. (6), the MFP for ionizing collisions has a minimum at approximately $\kappa=6$ (see Fig. 1). The time step is then taken to be 1% of the time taken to travel this critical distance under the applied field. Hence, the time step size τ is

$$\tau = \frac{1}{100}\sqrt{\frac{2\varphi}{x_{\mathrm{gap}}E_{\mathrm{app}}}}\left(\kappa_{\mathrm{min}}^{1/2}-1\right), \tag{8}$$

where κ_{min} is the value of κ at the minimum on the MFP curve. We believe that this gives us sufficient resolution of the curve without too heavy a computational overhead.

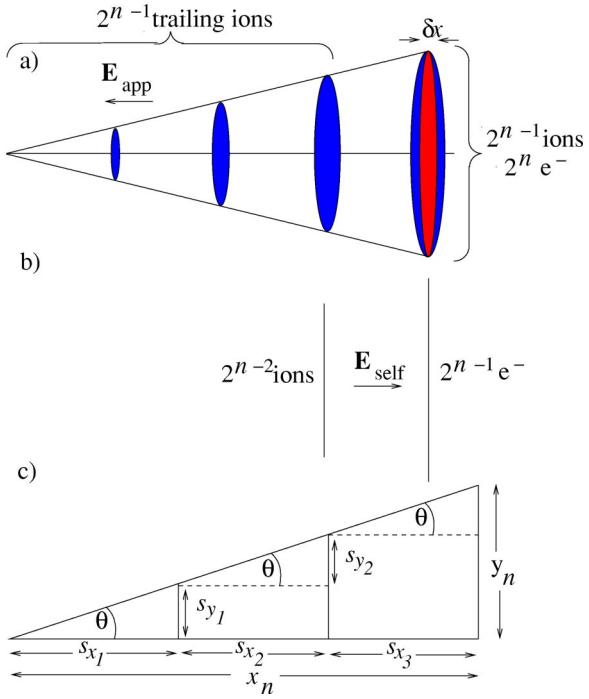

FIG. 2. Diagrams of an avalanche. (a) An idealized avalanche shows the tail of ions and the head of electrons and ions, (b) the approximation to a parallel plate system with twice as much charge on the negative plate as on the positive plate, (c) a schematic of the idealized avalanche.

C. Densities

Since the simulations presented here are two-dimensional (2D), the relationship between the particle densities we determine and the densities that enter Poisson's equation must be considered. In the earlier discussion of Poisson's equation, the nondimensionalized constant Λ included a linear density term $n_{1\mathrm{D}}$. This was required in the nondimensionalization of the densities, i.e.,

$$n^* = \frac{n_{3\mathrm{D}}}{n_{\mathrm{gas}}} = \frac{n_{2\mathrm{D}}n_{1\mathrm{D}}}{n_{\mathrm{gas}}}, \tag{9}$$

where n^* is the nondimensionalized density, $n_{2\mathrm{D}}$ is the model density with dimensions of m^{-2} (particles per grid cell), $n_{3\mathrm{D}}$ (right-hand side of Poisson's equation) is the true density with dimensions of m^{-3}, and n_{gas} is the characteristic density of the neutral gas.

A linear density is required to transform our 2D model density into a density of the same dimension as our characteristic density. This transformation is simply done by assuming that the number of electrons produced in our 2D Cartesian geometry simulation is the same as that produced in a 2D cylindrically symmetric geometry. For the purpose of this calculation the (x,y) coordinates of Cartesian geometry may be taken to be equivalent to the (r,z) coordinates of cylindrically symmetric geometry.

After n collisions the avalanche will have a head of 2^n electrons and 2^{n-1} ions, if starting with the one ion-electron pair. The other 2^{n-1} ions form a trailing tail where the num-

ber of ions increases by a power of 2 at each ion deposit, due to the size of the ion mobility compared to the electrons. This is shown schematically in an idealized situation in Fig. 2(a).

In cylindrically symmetric geometry the head of electrons would be spread amongst a volume $\pi r^2 \delta z_n$, hence, noting the equivalence to Cartesian coordinates, the density becomes

$$n_{3D} = \frac{2^n}{\pi y_n^2 \delta x_n}, \tag{10}$$

where y_n is the total y distance traveled by, and δx_n is the width of, the head of electrons.

But in this model this 3D volume becomes a 2D area, hence

$$n_{2D} = \frac{2^n}{2 y_n \delta x_n}. \tag{11}$$

Now using these two equations and the relation between them shown in Eq. (9), it can be shown that the linear density is given by

$$n_{1D} = \frac{n_{3D}}{n_{2D}} = \frac{2}{\pi y_n}. \tag{12}$$

As n is simply the number of collisions any value could be chosen, but it makes sense to choose a value that is representative of the system. Hence, the value of n used is the value at which the avalanche becomes a streamer.

We will say that the avalanche-to-streamer translation occurs at the moment the self-field of the avalanche becomes equal in magnitude to the applied field, and will refer to this as the ''streamer criterion.'' Using this definition the number of collisions for the streamer criterion to be met can be found, assuming that the distribution of charge is thin compared to the distance between collisions, s_x, for example, in a high-pressure neutral gas with a modest applied field. Further if all the ions at a distance greater than s_x from the electrons are ignored then the situation can be approximated to a parallel plate scenario, as shown in Figs. 2(a) and 2(b). Through Gauss's Law the self-field can be calculated, assuming that edge effects are ignored, and it is found to have the form

$$E_{self} = \frac{3\sigma}{2\varepsilon_0}, \tag{13}$$

where the direction of the field is from the ions to the electrons (in the opposite direction to that of the applied field) and σ is the charge per unit area of the plate. Note that to get the above form of the self-field a parallel plate capacitor with a σ given below is taken, and added to this field is the field from a single plate with negative charge of the same quantity on it. Thus the summation of the parallel plates and the single plate gives the situation shown in Fig. 2(b) where the negative plate has twice as much charge as the positive plate. Assuming that the avalanche is three dimensional as it would be in reality, and that the distributions of the plates of charge

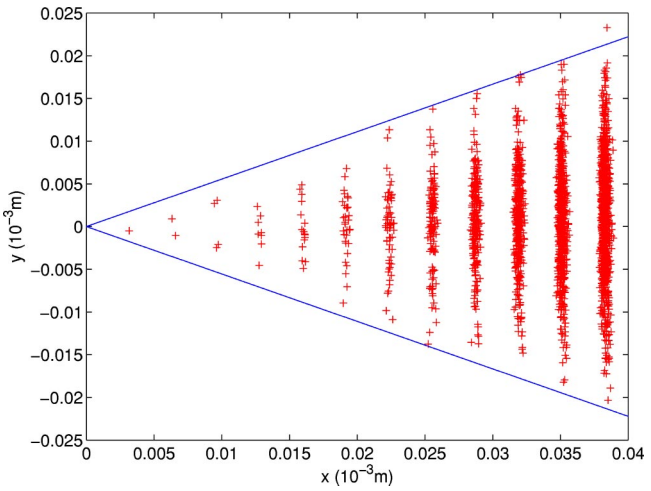

FIG. 3. Ion position during initial parts of an avalanche. The initial conditions here are the same as those stated in the text. Clearly visible is the banded structure of the ions, of which ≈5000 are shown. Note that all lie within lines of gradient ±0.55. More generally the angular spread is a consequence of collisional diffusion.

are circular, then expressions for σ and the self-field of the plates can easily be generated, hence

$$\sigma = \frac{2^{n-2} q}{\pi y_n^2}, \tag{14}$$

$$E_{self} = \frac{3 \times 2^{n-3} q}{\varepsilon_0 \pi y_n^2}, \tag{15}$$

where n is the number of collisions, q is the electric charge, and y_n is the total lateral distance traveled by the electrons between collisions.

Figure 2(c) shows that y_n is given by

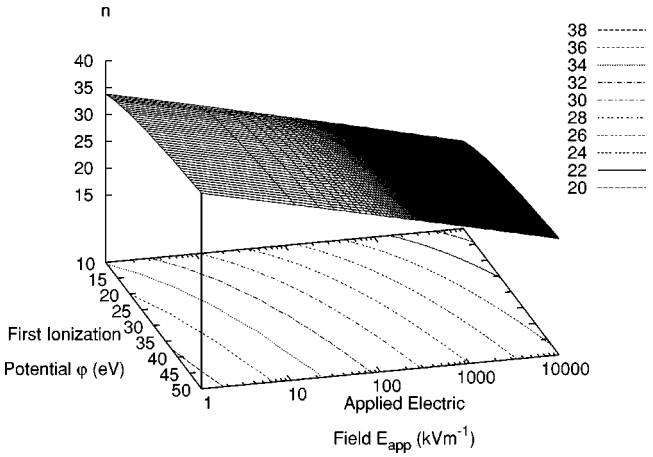

FIG. 4. Number of collisions required from an initial ion-electron pair, for various applied electric fields and first-ionization potentials, in order for the self-field generated to be equal in magnitude to the applied field.

$$y_n = \sum_{i=1}^{n} s_{y_i} = \tan\theta \sum_{i=1}^{n} s_{x_i}. \tag{16}$$

Combining this with the equations of motion it is easy to derive a recurrence relation for n:

$$E_{\text{self}}^{n} = \frac{3\times 2^{n-3} q}{\varepsilon_0 \pi \tan^2\theta \left(\sum_{i=1}^{n} s_{x_i} \right)^2}, \tag{17}$$

$$s_{x_n} = \frac{\varphi}{E_{\text{app}} + E_{\text{self}}^{n-1}}, \tag{18}$$

with

$$s_{x_1} = \frac{\varphi}{E_{\text{app}}}. \tag{19}$$

Hence the number of collisions at which the self-field is equal in magnitude to the applied field, i.e., n, can be calculated. The only input parameters needed for this are the first-ionization potential of the neutral gas and the applied field. The angle θ has to be deduced from the initial stages of an avalanche. It is given by the gradients of the lines encompassing the ion distribution. In this case, Fig. 3 shows that the encompassing lines have gradients of ± 0.55, i.e., a cone angle of $\approx 60°$.

The results of this recurrence relation for a wide range of applied fields and first-ionization potentials are shown in Fig. 4. For nitrogen gas ($\varphi = 15.58$ eV), and applied field of 5 MV/m, the self-field should be equal to the applied field after 21 collisions. Hence, the streamer criterion should be met when $2^{21} \approx 2.1\times 10^6$ ions and electrons are present in the avalanche.

These calculations yield a useful check on the numerical simulation, albeit only an order of magnitude result given the inherent assumptions.

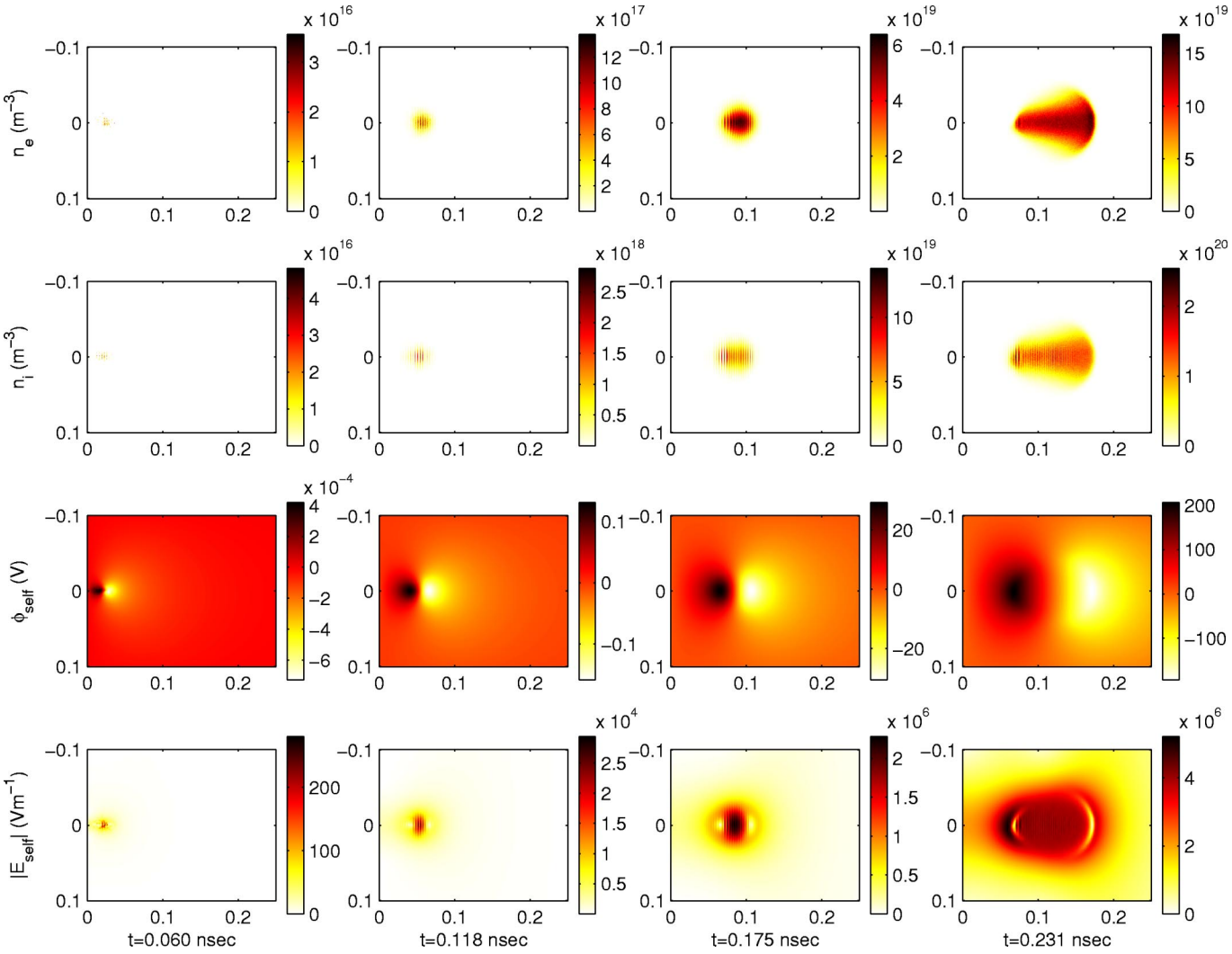

FIG. 5. Results of the high resolution simulation. The panels show, from the top, the electron density and ion density, both in units of m^{-3}, the self-potential in volts, and the magnitude of the self-field in V/m. The panel sequence from left to right shows the evolution of these properties in time and the x and y dimensions represent $x(10^{-3}$ m) and $y(10^{-3}$ m), respectively.

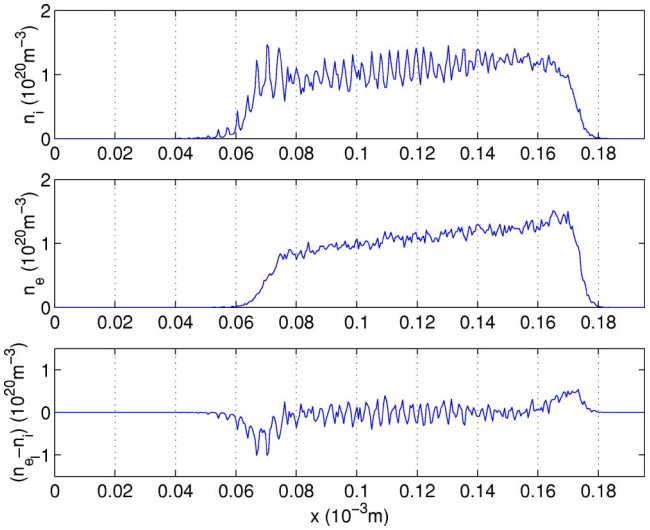

FIG. 6. A slice through the middle of the avalanche showing, from the top panel through to the bottom, the ion and electron distributions and the space charge $(n_e - n_i)$ at 0.229 ns. The banded structure is clearly present in the ions but not in the electrons. The space charge also has a clear banded structure.

D. Decimation

There is a limit on the number of particle trajectories that can be followed on any individual computer. This number is set by the available memory, e.g., 4×10^6 particles require ≈ 1 Gbyte (Gb) of memory. If this limit is reached before the required criteria for finishing the simulation are met, then a technique we term decimation can be employed: we randomly disgard half of the particles from the simulation, and give each of the remaining particles twice their former charge. The simulation then continues with fewer particles but with impaired resolution.

Note that the simulations presented here were conducted on individual processors of a 24 processor (Athlon 2200MP) Beowulf cluster, each with 1 Gb of random access memory. A parallel implementation [using Message Passing Interface (MPI)] is under development.

III. RESULTS AND DISCUSSION

The results of two simulations are presented. Both simulations use initial conditions that are common in streamer discharge simulations but at a higher resolution than generally used in such models. Results showing the evolution of a single avalanche and the interaction of several avalanches are presented. Both the simulations are started with a charge factor of $Q=1$ and concluded when the streamer criterion is met.

The conditions taken to be representative of previous work in this field are drawn from Ref. [12], namely, both simulations are evolved in atmospheric pressure N_2 gas in a parallel plate gap with a 5 MV m^{-1} applied field. The computational grid used was 1024×512 grid points, and the y dimension was always half that of the x dimension, the plate separation x_{gap}.

For both simulations the plate separation was 5 $\times10^{-4}$ m. This, along with the difference in coordinate systems, is the key difference to that of Ref. [12]. This allows us to achieve a higher resolution and although the boundaries are brought closer to the developing avalanche they are still sufficiently far away to have a minimal effect.

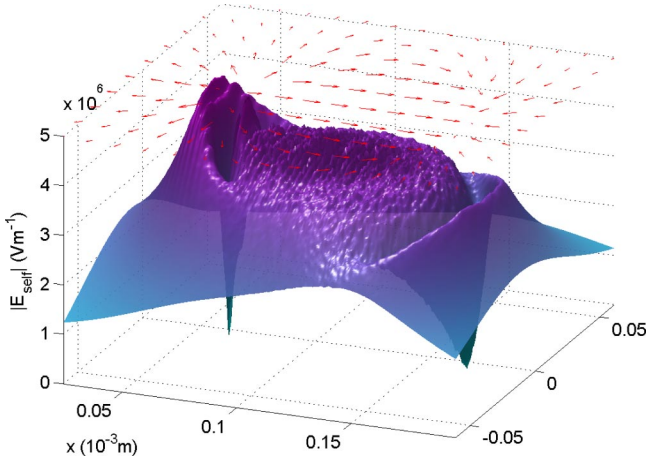

FIG. 7. A surface plot of the magnitude of the self-field, in which the banded structure of the ions can be seen. The arrows above the plot show the direction of the self-field. The time is 0.231 ns and corresponds to the final column in Fig. 5.

With this reduced plate separation we are able to achieve a resolution of ≈ 0.5 μm in both directions, but [12], with a plate separation ten times larger, achieves a resolution of 5 μm in the z direction and for the initial 0.1 cm of the r direction with a reduced resolution of 40 μm over the remaining region.

As these conditions are the same for both simulations the following parameters are fixed:

$$\Lambda = -3.69\times10^{-2}, \tag{20}$$

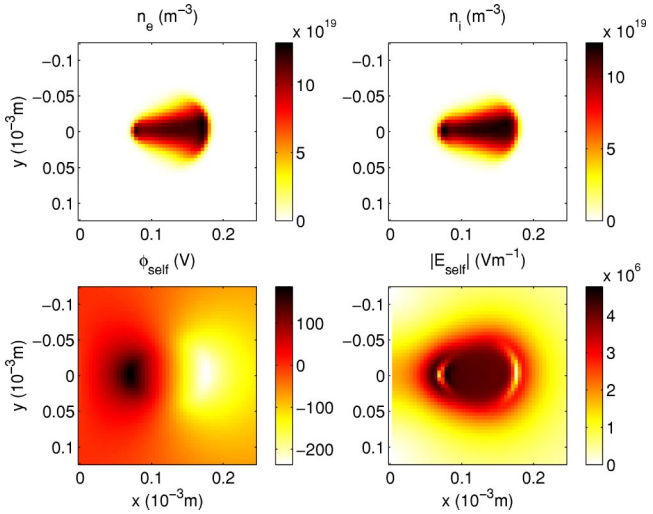

FIG. 8. The electron and ion density distributions, self-potential, and magnitude of the self-field at streamer criterion for a simulation using the same resolution and initial conditions as Ref. [12] and with the same initial seed positions as the single-avalanche case.

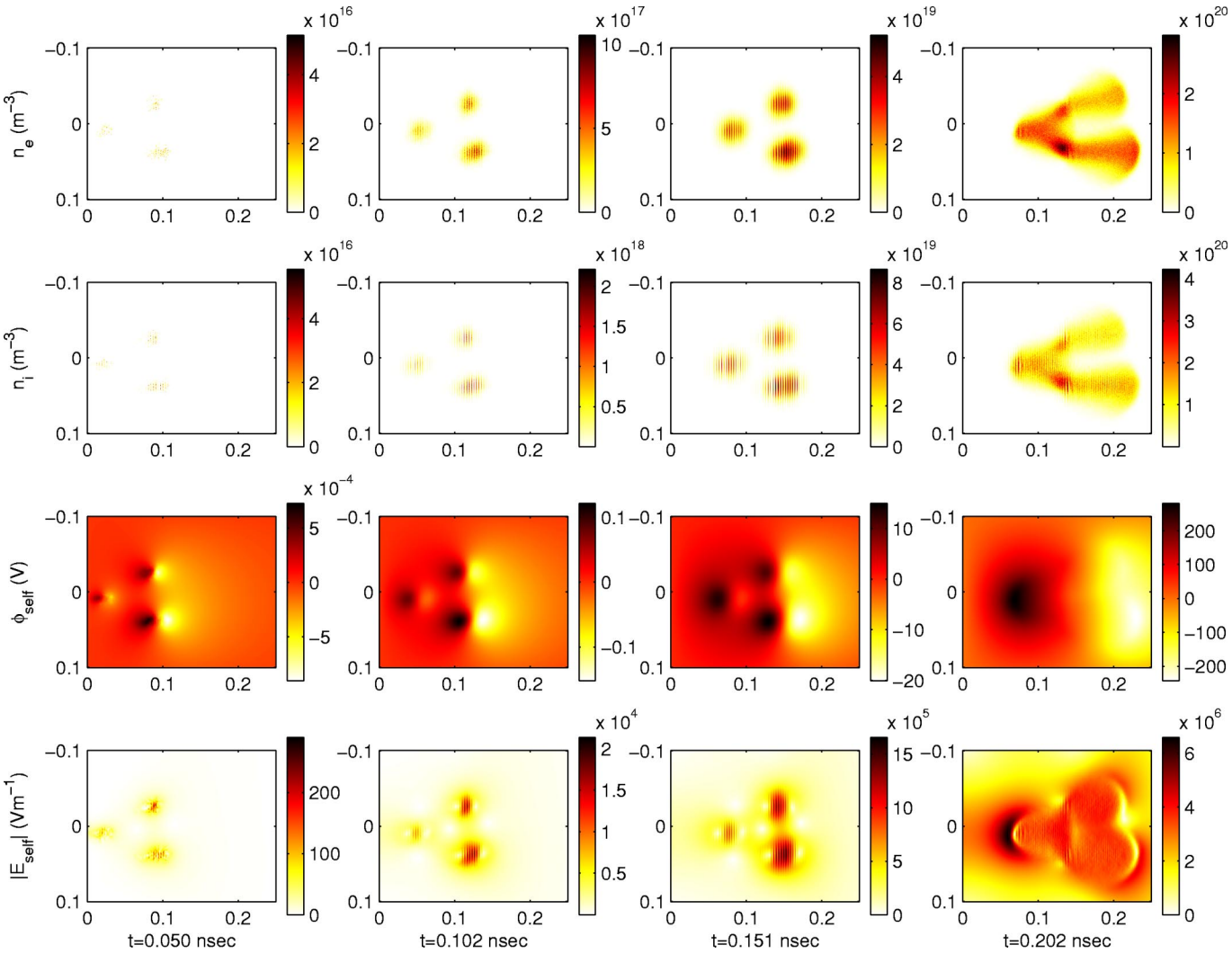

FIG. 9. The evolution of three initial seeds into interacting avalanches. The panels show, from the top, the electron density and ion density, both in units of m^{-3}, the self-potential in volts, and the magnitude of the self-field in V/m. The panel sequence from left to right shows the evolution of these properties in time and the x and y dimensions represent $x(10^{-3}$ m) and $y(10^{-3}$ m), respectively.

$$\tau = 1.67 \times 10^{-2}, \tag{21}$$

$$n_{1D} = 9730 \ \ \mathrm{m}^{-1}. \tag{22}$$

A. Single avalanche

The ion-electron pair is placed close to the cathode with the electron being 1 nm and the ion 2 nm from the cathode, both with $y=0$. In this simulation the streamer criterion was reached with $\approx 3.9 \times 10^6$ particles of each species but each with a charge factor of $Q=32$, a factor of 55 greater than our estimate.

The evolution of the electron and ion distributions, the self-potential, and magnitude of the self-field are shown in Fig. 5. The banded structure in the ion deposits is clearly visible even at the earliest time. However at late times, this banded structure becomes less distinct; consequently, the assumptions used to estimate the number of particles required at streamer criterion are no longer valid. This in part explains the discrepancy between the estimated and actual values. Also visible in the early stages of the avalanche is a banded structure in the electrons. This is simply a result of the doubling of the electron number in the ionization bands, which is smeared out by diffusion at later times. The self-field very quickly, in less than 0.23 ns, reaches the magnitude of the applied field, but in the opposite direction. Though in the initial stages the self-field is small in comparison to the applied field it can be seen that it plays a pivotal role in determining the dynamics of the system. By the time the streamer criterion is met the banded structure in the electron distribution has been replaced by a smooth, continuous distribution with a low density tail and a high density head which forms the ionization front, clearly seen in the middle panel of Fig. 6, which shows slices through the $y=0$ line of the electron and ion distributions and the space charge.

Figure 6 also clearly shows the banded structure present in the ions. The distance between the peaks is characteristic of the distance between ionizing collisions, that is, the distance required for an electron to reach threshold energy for ionization and then undergo an ionizing event. The banded

structure is not present in the electron distribution and hence the banded structure in the ions carries on through to the space charge also shown. Consequently, this structure is present in the self-potential and the self-field, the magnitude of which is shown in Fig. 7. The self-field in the interior region of the avalanche, the region behind the ionization front, has a magnitude almost equal but opposite in direction to the applied field. The charges in this region experience comparatively small fields.

From Figs. 5 and 6 it is clear that the spatial distributions of the charged particles are far from being consistent with a circular Gaussian when the streamer criterion is met. Moreover, there is a nonzero space charge which leads to a significant self-field, which are evolving self-consistently (the streamer is simply the continued development of this self-consistent structure), and play a key role in determining the dynamical evolution of the system. Even at a lower resolution this analysis still holds, as shown in Fig. 8, where the results of a simulation performed at the same resolution of Ref. [12] are shown.

The non-Gaussian particle distributions, of both species, are in disagreement with the initial particle distributions of most fluid models. In addition, the avalanche progresses a considerable distance ($\sim$0.17 mm) before the streamer criterion is met and the particle density is as high as 10^{20} m^{-3} (the starting density for the simulations of Ref. [12]). As a result, it is not possible for a streamer to begin on the cathode. Furthermore, it is commonly assumed in fluid model that the electron and ion distributions are initially identical, leading to a zero space charge, a zero self-potential, and a zero self-field. In all the simulations presented here this is clearly not the case. As the particle distributions of each species differ there is a finite space charge, which ultimately produces a highly significant self-field. This is in disagreement with the initial assumptions of most fluid models.

B. Multiple avalanches

Having seen that significant self-fields can be developed in the avalanche phase, it is possible that multiple avalanches could significantly interact with each other before the onset of the streamer criterion. In order to investigate this a second simulation was undertaken. The applied conditions were the same as in the single-avalanche case. However, three initial seeds were used. These were located at $(10^{-4},0)$, $(60,35)$, and $(60,-35)$, all measured in microns. With these positions the interaction of two avalanches evolving at the same y position and the effect of an avalanche evolving through the trailing ions of previous avalanches could be investigated.

Figure 9 shows the evolution of the electron and ion distributions and the self-potential and magnitude of the self-field, all at the same times as the single-avalanche case. In the early stages all three seeds evolve into a similar avalanche, as their interaction with each other is not yet important in determining their dynamics. However, as the avalanches grow so does their interaction.

The interaction of the two leading avalanches introduces a slight skewness, compared to that of the single-avalanche case, to their ionization fronts, shown by the black contours

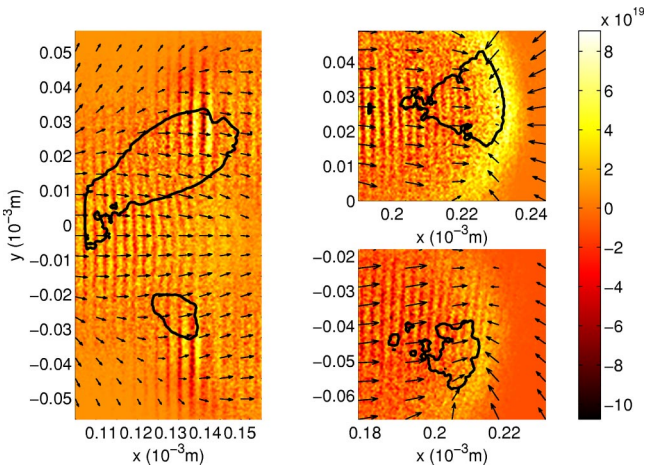

FIG. 10. A closeup of the trailing and leading ionization fronts are shown. The image is of the space charge $n_e - n_i$ in m^{-3}, with the arrows showing the direction and magnitude of the self-field. Note that the applied field has a magnitude equal to the longest arrow and points from a higher to lower x direction. Finally, contours showing the locations of the ionization fronts are denoted by a thick black line. This contour is of an electron density equal to 70% of the maximum electron density in the region plotted.

in the right-hand panels of Fig. 10. This figure shows the direction and magnitude of the self-field via the arrows, the location of the leading ionization fronts by the black contours, and the space charge in the background image, where we can still see the banded structure. It is seen that the leading edge of the leading ionization fronts experiences very little self-field. That is, they are exposed almost solely to the applied field and so are continually accelerated and are able to cause ionization. However, behind these ionization fronts, in the interior region, there is again very little net field, just as in the single-avalanche case.

The two leading ionization fronts just continue to propagate in a similar fashion to their previous propagation. Indeed, if the simulation were allowed to continue it is possible that the two leading ionization fronts would merge into one that would be of similar shape to that of the single-avalanche case. This scenario would most likely be initially seen in the potential, where it is seen from the evolution that the three distinct potential fields of the three avalanches merge into one of similar shape to the single-avalanche case, suggesting that the leading two avalanches are merging into one.

However, for the trailing avalanche the ionization front is split, easily seen in the left hand panel of Fig. 10. Clearly what should have been one contour representing the one ionization front has been split in two. Further, as the net space charge in these regions is small it can be deduced that the ionization front of electrons has been split by the trailing ions, deposited by the two leading avalanches, that we know are present from the single-avalanche case.

The key difference this makes is that, compared to the two leading ionization fronts propagating into neutral gas, the trailing ionization front is traveling into plasma. The field in this region is opposite and almost equal to the applied field. Hence, the trailing ionization fronts are traveling in a region with approximately no net field. In this case their dynamics

will be influenced almost solely by the local charge population, whereas the dynamics of leading ionization fronts are determined by the applied field.

IV. CONCLUSIONS

A 2D particle code capable of modeling self-consistently an avalanche from the first ion-electron pair up to streamer conditions has been produced and is reported here. The results from this code demonstrate that the initial conditions usually adopted for fluid models of streamer discharges are unrealistic because of their neglect of the self-field.

The particle code has shown that the streamer criterion is met not on the cathode, as is commonly assumed in some fluid simulations, but at a noninsignificant distance from the cathode. Furthermore, the particle code has shown that the charged-particle distributions at streamer onset are highly non-Gaussian and differ from each other. The consequent nonzero space charge yields a significant self-field which strongly influences the subsequent evolution of the streamer.

These self-fields develop rapidly and account for significant interaction between avalanches. The onset of plasma behavior can be seen by the ability of space charge to shield itself from externally applied electric fields. It is clear that a self-consistent particle model is vital for accurate quantitative modeling of discharge evolution.

Note that no density ''spike'' appears at the streamer onset, in contrast to some fluid simulations in the literature. Instead the density distribution here is self-consistent, rather than reflecting the persistence of the inappropriate initial conditions assumed in some fluid models. Future computational work in the fluid regime ought to take this into account.

Parallel implementations (under MPI) of this 2D code and a full 3D particle model are being developed and results will be presented shortly.

ACKNOWLEDGMENTS

It is a pleasure to acknowledge valuable discussions with Dr. H. E. Potts. This work was performed under EPSRC Grant No. GR/N32198/01.

[1] H. Raether, Z. Phys. **112**, 464 (1939).
[2] H. Raether, Arch. Elektrotech. (Berlin) **34**, 49 (1940).
[3] L.B. Loeb and J.M. Meeks, J. Appl. Phys. **11**, 438 (1964).
[4] A.J. Palmer, Appl. Phys. Lett. **25**, 138 (1974).
[5] N.St.J. Braithwaite, Plasma Sources Sci. Technol. **9**, 517 (2000).
[6] G.G. Lister, J. Phys. D **25**, 1649 (1992).
[7] F.M. Penning, *Electrical Discharges in Gases* (Philips' Technical Library, London, 1957).
[8] J.D. Cobine, *Gaseous Conductors Theory and Engineering Applications* (Dover, New York, 1958).
[9] F. Llewellyn-Jones, *The Glow Discharge* (Wiley, New York, 1966).
[10] J.M. Meek and J.D. Craggs, *Electrical Breakdown of Gases* (Oxford University Press, Oxford, 1953).
[11] M.A. Lieberman and A.J. Lichtenberg, *Principles of Plasma Discharges and Materials Processing* (Wiley, New York, 1994).
[12] P.A. Vitello, B.M. Penetrante, and J.N. Bardsley, Phys. Rev. E **49**, 5574 (1994).
[13] S.K. Dhali and P.F. Williams, J. Appl. Phys. **62**, 4696 (1987).
[14] U. Arrayas, M. Ebert, and W. Hundsdorfer, Phys. Rev. Lett. **88**, 174502 (2002).
[15] A.A. Kulikovsky, J. Phys. D **27**, 2564 (1994).
[16] S.K. Dhali and P.F. Williams, Phys. Rev. A **31**, 1219 (1985).
[17] A.A. Kulikovsky, J. Phys. D **27**, 2556 (1994).
[18] Won J. Yi and P.F. Williams, J. Phys. D **35**, 205 (2002).
[19] P. Tardiveau, E. Marode, A. Agneray, and M. Cheaib, J. Phys. D **34**, 1690 (2001).
[20] A. Fiala, L.C. Pitchford, and J.P. Boeuf, Phys. Rev. E **49**, 5607 (1994).
[21] J.P. Boeuf, J. Appl. Phys. **63**, 1342 (1988).
[22] W.H. Press, S.A. Teukolsky, W.T. Vettererling, and B.P. Flannery, *Numerical Recipies in Fortran*, 2nd ed. (Cambridge University Press, Cambridge, 1966).
[23] Y.K. Kim, J. Res. Natl. Inst. Stand. Technol. **97**, 689 (1992).
[24] See http://physics.nist.gov/PhysRefData/
[25] R.B. Brode, Rev. Mod. Phys. **5**, 257 (1933).
[26] E.W. McDaniels, *Atomic Collisions: Electron and Photon Projectiles* (Wiley, New York, 1989).